Title	Characterization of an extendable multi-leaf collimator for clinical electron beams
Author(s)	O'Shea, Tuathan P.; Foley, Mark J.
Publication Date	2011
Publication Information	O'Shea, TP,Ge, YY,Foley, MJ,Faddegon, BA (2011) 'Characterization of an extendable multi-leaf collimator for clinical electron beams'. Physics In Medicine And Biology, 56 :7621-7638.
Publisher	Institute of Physics
Link to publisher's version	http://dx.doi.org/10.1088/0031-9155/56/23/018
Item record	http://hdl.handle.net/10379/4180
DOI	http://dx.doi.org/DOI 10.1088/0031-9155/56/23/018

Characterisation of an Extendable Multi-leaf Collimator for Clinical Electron Beams

Tuathan P O'Shea[1], Yuanyuan Ge[3], Mark J Foley[1]

and Bruce A Faddegon[2]

[1] School of Physics, National University of Ireland Galway, University Road, Galway, Ireland

[2] University of California San Francisco Comprehensive Cancer Center, 1600 Divisadero Street, San Francisco, CA 94143-1708, USA

[3] Central Clinical School, University of Sydney, Sydney, NSW 2006, Australia

E-mail: bfaddegon@radonc.ucsf.edu

Abstract

An extendable x-ray multi-leaf collimator (eMLC) was investigated for collimation of electron beams on a linear accelerator. The conventional method of collimation using an electron applicator is impractical for conformal, modulated and mixed beam therapy techniques. An eMLC would allow faster, more complex treatments with potential for reduction in dose to organs-at-risk and critical structures. The add-on eMLC was modelled using the EGSnrc Monte Carlo code and validated against dose measurements at 6 – 21 MeV with the eMLC mounted on a Siemens Oncor linear accelerator at 81.6 cm source-to-collimator distance. Measurements and simulations at 8.4 – 18.4 cm air-gaps showed agreement of 2% / 2 mm. The eMLC dose profiles and percentage depth dose curves were compared with standard electron applicator dosimetry. The primary differences were a 0.12 ± 0.03 cm wider penumbra and up to 4.2% reduction in the build-up dose at 0.5 cm depth, with dose normalised on the central axis. The eMLC leaves, which were 7 cm thick, contributed up to 6.3% scattered electron dose at the depth of maximum dose for a 10 × 10 cm^2 field, with the thick leaves effectively eliminating bremstrahlung leakage. A Monte Carlo calculated wedged shaped dose distribution generated with all six beam energies

matched across the maximum available eMLC field width demonstrated a therapeutic (80% of maximum dose) depth range of 2.1 – 6.8 cm. Field matching was particularly challenging at lower beam energies (6 – 12 MeV) due to the wider penumbrae and angular distribution of electron scattering. An eMLC isocentric electron breast boost was planned and compared with the conventional applicator fixed source-to-surface distance (SSD) plan, showing similar target coverage and dose to critical structures. The mean dose to the target differed by less than 2%. The low bremsstrahlung dose from the 7 cm thick MLC leaves had the added advantage of reducing the mean dose to the whole heart. Isocentric delivery using an extendable eMLC means that treatment room re-entry and repositioning the patient for SSD set-up is unnecessary. Monte Carlo simulation can accurately calculate the fluence below the eMLC and subsequent patient dose distributions. The eMLC generates similar dose distributions to the standard electron applicator but provides a practical method for more complex electron beam delivery.

1 INTRODUTION

Electron beam therapy is typically administered under fixed source-to-surface distance (SSD) conditions using an electron applicator and a custom lead alloy insert. It is a common modality for treating superficial tumours of the chest wall. Clinical evidence shows the benefit of boosting the breast tumour excision site with electrons, for example (Bartelink et al. 2001). The potential for electron breast boost geographic misses has been identified, highlighting the need for accurate tumour bed localisation on a daily basis (Fraser et al. 2010). The potential for dose calculation inaccuracies due to approximations made by commercial planning software has also been shown (Coleman et al. 2005). In addition to the accuracy improvements introduced by using Monte Carlo-based dose calculation (Chetty et al. 2007), electron beam therapy would also benefit from more accurate and precise techniques of delivery.

Complex and precise electron dose delivery is an active area of research, particularly the use of modulated electron and mixed (x-ray and electron) beam therapy techniques (Li et al. 2000, Ma et al. 2003, Gauer et al. 2010, Surucu et al. 2010, Alexander et al. 2011). Modulated electron beam

therapy provides a method of conformal treatment and has been shown to provide a reduction in dose to distal organs-at-risk and critical structures (Ma et al. 2003, Jin et al. 2005). Conventional methods for electron beam collimation are labour and time intensive in their construction and are considered inadequate for use in the sequential delivery of multiple complex fields. A number of authors have investigated the use of either the x-ray multi-leaf collimator (pMLC) or a dedicated electron multi-leaf collimator (eMLC) for un-modulated or modulated electron beam delivery (Lee et al. 2000, Hogstrom et al. 2004, Gauer et al. 2008, Al-Yahya et al. 2007, Klein et al. 2008).

Lee et al. (2000) investigated two methods of electron beam collimation: (1) using the existing photon multi leaf collimators (pMLC) in a helium atmosphere to reduce in-air electron scatter, and (2) using a MLC specifically designed for electron beam collimation located at the level of the last scraper of the 25 × 25 cm^2 applicator on a Varian accelerator. Significant improvements, particularly in the dose profile penumbra, were reported when the treatment head air was replaced with the helium based system. Simulations were also performed on an electron specific MLC with unfocused tungsten leaves 1.5 cm thick and 0.5 cm wide which provided sufficient collimation for modulated electron fields.

Hogstrom et al. (2004) proposed a retractable eMLC used for un-modulated or intensity modulated therapy which could (a) retract to 63 cm source-to-collimator distance (SCD) for arc therapy, or deploy to (b) 80 cm or (c) 90 cm SCD for isocentric and SSD set-ups, respectively. The eMLC design was capable of treatment which was equivalent to that delivered by a standard cerrobend insert, due to similar dosimetric properties (up to 3% difference in the build-up region of the percentage depth dose curve). The benefits of isocentric electron treatment were discussed, particularly in breast and head and neck (e.g. posterior neck region) cases when combined with isocentric x-ray beams. Advantages would include faster treatments due to no treatment room re-entry and no need to reposition the couch.

Gauer et al. designed, evaluated (2006) and characterised (2008) an add-on eMLC with interchangeable distance holders for variable SCD (72 cm or 84 cm) and isocentric delivery on a Siemens Primus accelerator. The final eMLC design consisted of two banks of 24 brass leaves with height and width of 1.8 cm and 0.6 cm, respectively. Attachment and gantry stability was evaluated and found to result in a maximum displacement of 0.6 mm. The dosimetric properties, including field size dependence, field abutment and leakage, of the eMLC were evaluated. Dose profiles and percentage depth dose curves were compared with that of the standard applicator demonstrating a 0.8 – 0.4 cm larger penumbra and build-up effect (limited to energies up to 14 MeV).

Klein et al. (2008) used the 120 leaf pMLC on a Varian accelerator to develop and evaluate narrow (1 - 10 cm) beam segments for modulated electron treatments at 6 – 20 MeV using Monte Carlo methods. The study employed shorter source-to-surface distances (70 - 85 cm) in order to improve the beam penumbrae. Monte Carlo planning was then performed on idealised phantom and clinical cases for segmented and dynamic leaf delivery (Klein et al. 2009). Sparing of distal organs at risk was reported, however, it was also noted that the use of shorter SSDs may be clinically impractical due to potential collisions and some treatment sites may need to be treated at larger SSD (>75 cm), degrading the penumbra and plan resolution.

Jin et al. (2008) investigated modulated electron therapy using the pMLC on Siemens Primus accelerator. A Monte Carlo method of inverse planning was developed. Again, a shortened SSD (60 cm) was employed to improve the penumbra of 6 – 15 MeV electron beams. A treatment consisting of 22 segments was planned and delivered on a breast phantom with measurements and simulations reported to agree to 2% / 1 mm.

It can be concluded that the current commercially available x-ray MLCs are generally unsuitable for electron beam collimation at nominal SSD (100 cm). Electron beams should ideally be collimated (in air) within 10 cm of the skin surface to reduce the size of the penumbra and maintain

beam flatness, especially at lower (more widely scattered) beam energies. This would also aid matching and dose uniformity at beam junctions in modulated or abutted fields (Steel et al. 2009, Eldib et al. 2010). Studies which utilised the pMLC for electron beam collimation utilised a shortened SSD in order to improve the penumbra. A dedicated retractable eMLC may be the optimal method for electron beam collimation. This could be placed in close proximity (5 – 10 cm) to the patient to provide an adequate penumbra and resolution and then remotely retracted to allow concomitant x-ray treatment.

This paper is concerned with characterisation of an extendable x-ray MLC for collimation of the full set of clinical electron beams available (6 – 21 MeV) on a linear accelerator. Previous studies (e.g. Hogstrom et al. 2004, Gauer et al. 2008) have generally investigated thinner, lower atomic number MLCs dedicated to electron beam delivery. The MLC was modelled in EGSnrc/MCRTP (Faddegon et al. 1998) and validated against water phantom dose measurements. The dose profile penumbrae and electron scattering were evaluated and dosimetric properties were compared with the standard applicator. Potential concerns, including bremsstrahlung x-ray dose and dose inhomogeneity in abutting fields of differing energy were investigated. The energy modulation possibilities and variation in therapeutic range achievable were examined for an wedge shaped dose distribution. A concomitant eMLC- collimated electron breast boost was planned using Monte Carlo calculations to demonstrate the isocentric treatment capabilities of the eMLC. The resulting plan was compared with the fixed SSD approach using a standard applicator.

2 MATERIALS AND METHODS

2.1 Extendable Multi-leaf Collimator

A TiGRT Dynamic Multi-leaf Collimator (DMLC H, LinaTech, Sunnyvale, CA, USA) was mounted on a Siemens Oncor linear accelerator (Siemens OCS, Erlangen, Germany) using 30 cm steel extenders at

a SCD (side of the collimator closest to the patient) of 81.6 ± 0.1 cm. The eMLC was centred to within 0.03 cm of the central axis. It is composed of two banks of 51 tungsten leaves which have a height (thickness) of 7 cm along the beam axis. The central 19 leaves in each bank have a width of 0.2 cm (to the nearest millimeter) perpendicular to leave motion. The outer 32 leaves of each bank are 0.3 cm wide. The maximum physical field size is 15.0 × 17.0 cm^2. The leaves provide full over-travel and have a position uncertainty of 0.05 cm. The eMLC replaced the accessory rails and electron applicator, and in its full clinical implementation could be remotely retractable and deployed from approximately 59 – 95 cm SCD.

2.2 Dose Measurements

Dose profiles and percentage depth dose curves were measured in a water phantom (IBA Dosimetry, Bartlett, TN, USA) for 6, 9, 12, 15, 18 and 21 MeV electron beams, 71.6 cm and 81.6 cm SCD and 90 cm and 100 cm SSD. These SSDs represented air-gaps of 8.4 cm and 18.4 cm from the lower surface of the eMLC to water surface, respectively. Dose profiles were measured with a CC13 thimble chamber and an EFD diode for nominal 3 × 3, 10 × 10 and 20 × 20 cm^2 field sizes at several depths including R_{max} and a few centimeters beyond the practical range (R_x). Percentage depth dose curves were measured with the EFD diode. To evaluate the effects of the eMLC on clinical beams, the dosimetric properties of the eMLC collimated fields were compared with those of the standard 10 × 10 cm^2 electron applicator (95 cm SCD) at 100 cm SSD.

A wedge shaped dose distribution was planned using Monte Carlo simulation to demonstrate the eMLC energy modulation possibilities, and variation in target depth coverage achievable. The plan used a single isocentre and the six available electron beam energies (6 - 21 MeV) matched across the maximum available eMLC field size. To ensure that scatter from the eMLC banks was adequately modelled, dose profiles were measured (at 1 cm depth) for the the six adjacent fields

collimated with the eMLC (one for each beam energy) for comparison with the simulated wedge profile components.

In order to maintain the highest dose resolution, while potentially reducing the number of leaves and complexity of the eMLC, the optimal leaf width was also investigated. For this investigation, dose profiles were measured with 2, 4, 6 and 8 (0.2 cm) leaves alternating open or closed. The dose was normalised to the maximum in the open field segment and the subsequent reduction in dose under the closed leaf segment was evaluated.

Relative output factors were measured using an EFD diode and digital electrometer (Model 35614: Keithley Instruments, Cleveland, OH) at 90 cm and 100 cm SSD with the eMLC defining 2 × 2, 3 × 3, 10 × 10 and 20 × 20 cm^2 nominal field sizes and the detector at the depth of maximum dose for each field size.

2.3 Monte Carlo Simulation

Monte Carlo simulation was performed with the EGSnrc/BEAMnrc (Rogers et al. 1995) and MCRTP (Faddegon et al. 1998) codes. The treatment head above the eMLC was previously modelled to high accuracy for 6 – 21 MeV electron fields and included simulation of the fringe magnetic field from the bending magnet (Faddegon et al. 2009, O'Shea et al. 2011). The eMLC was modelled in the EGSnrc user code MCRTP for 71.6 cm and 81.6 cm source-to-collimator distances (SCD) and 90 cm and 100 cm SSD for characterisation and comparison with measured data. Tungsten with a density of 19.3 g cm^{-3} was used to model the leaf material. The treatment head was also modelled with standard 10 × 10 cm^2 electron applicator for comparsion of applicator and eMLC dosimetric properties. The Electron (ECUT/AE) and photon (PCUT/AP) cut-offs were 0.7 MeV and 0.01 MeV, respectively. The PRESTA-I boundary-crossing algorithm was used in MCRTP. The electron step algorithm was PRESTA-II

(Kawrakow and Rogers 2000). The default maximum step size (SMAX) of 5 cm was used. The maximum fractional energy loss per step (ESTEPE) was set to 0.25 (default). Dose-to-water was calculated in a phantom containing 2.0 × 2.0 × 1.0 mm^3 voxels as part of the eMLC simulation. The EGSnrc particle tracking variable LATCH was used to extract scattered electron and contaminant bremsstrahlung x-ray dose components for water phantom dose calculations.

2.4 Patient Plan

An electron breast boost was planned by Monte Carlo simulation using the methodology previously described and experimentally validated (using RANDO® phantom measurements) by Coleman et al. (2005). 3D dose distributions were calculated on patient anatomical data in MCRTP for a conventional (SSD) applicator boost and an isocentric boost using the extendable eMLC. Table 1 compares the two plan configurations. The eMLC plan utilised the same isocentre as the tangential (whole breast irradiated) x-ray fields, while the applicator plan required a shift from the x-ray isocentre. The displacement of the eMLC leaves (field offset) in the direction of motion (Δx) and perpendicular to the the direction of motion (Δy) required to maintain the same treatment field position (on the patient skin) as the applicator plan was calculated using:

$$\Delta x = \cos(\theta)(\Delta LAT) + \sin(\theta)(\Delta AP) \qquad (2.1)$$

$$\Delta y = -\Delta SI \qquad (2.2)$$

Table 1. Comparison of conventional applicator SSD and eMLC isocentric electron breast boost plan configurations. The isocentre shift indicates the treatment couch repositioning required for the applicator plan. The field offset was the displacement of the eMLC leaves in the direction of motion (Δx) and perpendicular to the the direction of motion (Δy) required to maintain the same treatment field position (on the patient skin) as the applicator plan.

	Applicator	eMLC
Mode	SSD	Isocentric
Energy [MeV]	18	18
Iso. shift (*ΔLAT, ΔAP, ΔSI*) [cm]	11.48, 5.72, 0.60	~
Gantry angle (θ) [°]	300	300
SSD [cm]	105.0	92.2
SCD [cm]	95.0	82.2
Air-gap [cm]	10.0	10.0
Field offset (*Δx, Δy*) [cm]	~	0.78, -0.60

The 3D dose distribution calculated in MCRTP was imported into the PlanUNC planning software (Schreiber et al. 2006) which was used to compare isodose distributions and dose volume histograms (DVH) for the target (tumour bed), right lung and whole heart. DVHs were quantitatively compared by $D95_{CTV}$: the minimum dose covering 95% of the target volume, $V20_{lung}$ (cm^3): the lung volume containing at least 20% of the prescribed dose, $V10_{heart}$ (cm^3): the heart volume containing at least 10% of the prescribed dose and also the mean dose to each of these structures. The plans were also delivered to a water phantom for comparison of simulated dose profiles and percentage depth dose curves.

3 RESULTS AND DISCUSSION

3.1 Dosimetric Characteristics and Model Validation

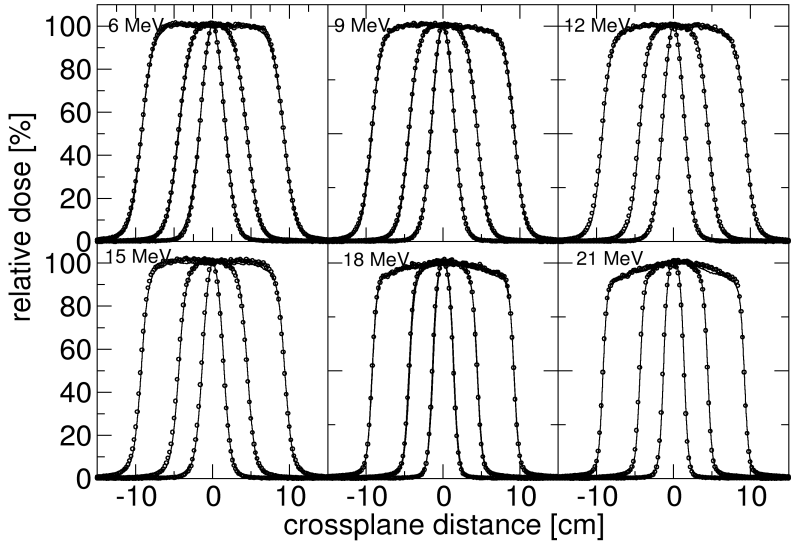

Figure 1. Cross-plane profiles for 2×2, 10×10 and 20×20 cm^2 nominal field sizes collimated with eMLC. 6, 9 and 12 MeV (top row left to right). 15, 18 and 21 MeV (lower row left to right). Monte Carlo calculations (points) are compared with diode measurements (lines).

Measured water phantom dose distributions for fields collimated with the eMLC were compared to Monte Carlo simulations at 90 cm and 100 cm SSD. Figure 1 shows the comparison of measured and simulated dose profiles for nominal 3 × 3, 10 × 10 and 20 × 20 cm^2 square fields at 100 cm SSD. Measured and simulated dose profiles and percentage depth dose curves showed agreement of 2% / 2 mm, and generally better, at both SSDs.

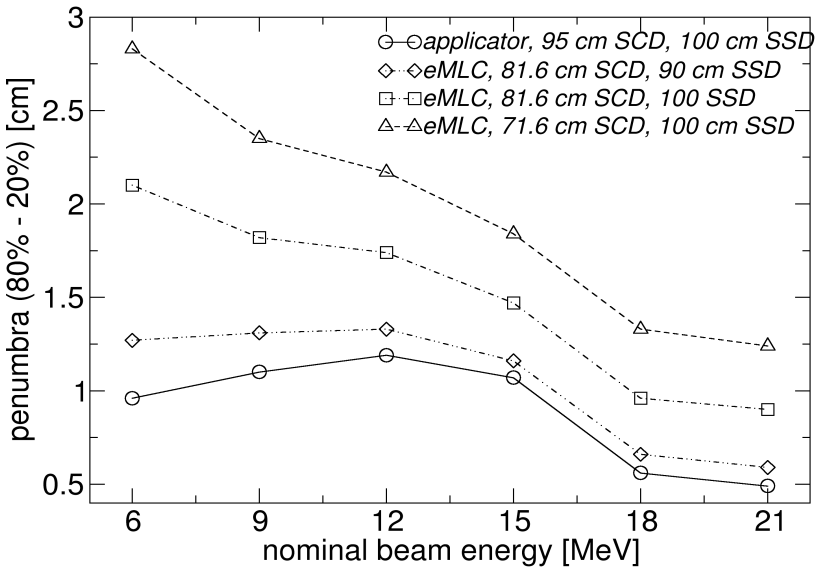

Figure 2. Comparison of applicator and eMLC dose profile penumbrae for various eMLC source-to-collimator and source-to-surface distances.

Figure 2 compares the penumbra widths (80% - 20% of relative dose) of the standard 10 × 10 cm^2 applicator and the 10 × 10 cm^2 eMLC field for 6 – 21 MeV electron beams. The penumbral widths for three different eMLC configurations: (i) 81.6 cm SCD, 90 cm SSD (8.4 cm airgap), (ii) 81.6 cm SCD, 100 cm SSD (18.4 cm airgap) and (iii) 71.6 cm SCD, 100 cm SSD (28.4 cm airgap) are included. The eMLC penumbra was wider in all cases, however, it was within 0.3 – 0.1 cm (6 – 21 MeV) of the applicator penumbra when the airgap was reduced to configuration (i) above. This demonstrated that the difference in applicator and eMLC penumbra was mainly the result of the difference in airgap between the collimator and phantom surface.

Table 2. Dose profile parameters for 10 × 10 cm² field and 100 cm SSD (with eMLC parameters at 90 cm SSD included in italics). Dosimetric and therapeutic field widths are the distances between the 50% and 80% off-axis doses relative to the central axis dose, respectively. The penumbra is the distance between 20% and 80% off-axis doses.

Dose profile parameters [cm]	Applicator						eMLC					
	energy [MeV]						*energy [MeV]*					
	6	*9*	*12*	*15*	*18*	*21*	*6*	*9*	*12*	*15*	*18*	*21*
Dosimetric field width	10.18	10.28	10.35	10.39	10.24	10.22	10.30	10.35	10.41	10.42	10.25	10.22
							9.94	*9.99*	*10.05*	*10.06*	*9.84*	*9.81*
Therapeutic field width	9.10	9.19	9.22	9.39	9.67	9.71	8.25	8.49	8.65	8.97	9.30	9.32
							8.83	*8.85*	*8.86*	*9.00*	*9.20*	*9.22*
Penumbra	0.97	1.11	1.19	1.08	0.57	0.51	2.13	1.84	1.76	1.47	0.96	0.91
							1.27	*1.31*	*1.34*	*1.19*	*0.66*	*0.59*

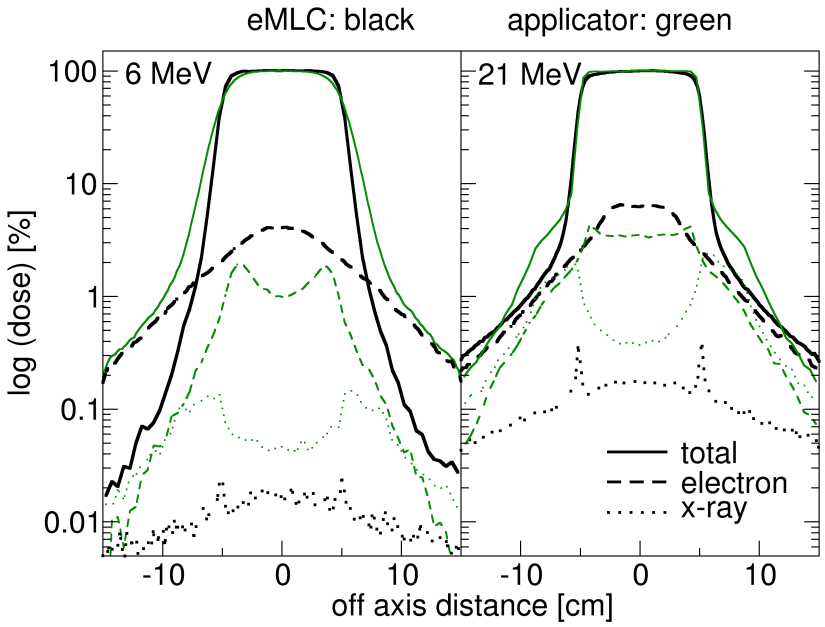

Figure 3. Dose profiles for 6 and 21 MeV electron beams showing dose contribution from total electron beam and scattered electrons and bremsstrahlung X-rays from eMLC at 81.6 cm SCD and applicator at 95 cm SCD for 100 cm SSD.

The clinically applicable R_{max} dose profile parameters for the 10 × 10 cm^2 applicator and eMLC (SCD = 81.6 cm) fields at 100 cm SSD are compared in table 2. The dose profiles of the eMLC had lower off-axis dose fall-off as quantified by the penumbra and therapeutic field (distance between 80% relative dose points) widths. The penumbra of the 6 - 21 MeV beams was 1.2 - 0.4 cm wider and the therapeutic field widths were 0.85 – 0.4 cm narrower than those of the 10 × 10 cm^2 applicator. Table 2 also includes the eMLC dose profile parameters at 90 cm SSD which are of more relevance to isocentric electron beam delivery. At 90 cm SSD the eMLC therapeutic field widths and penumbrae are within 0.5 cm and 0.3 cm of the corresponding applicator parameters, respectively.

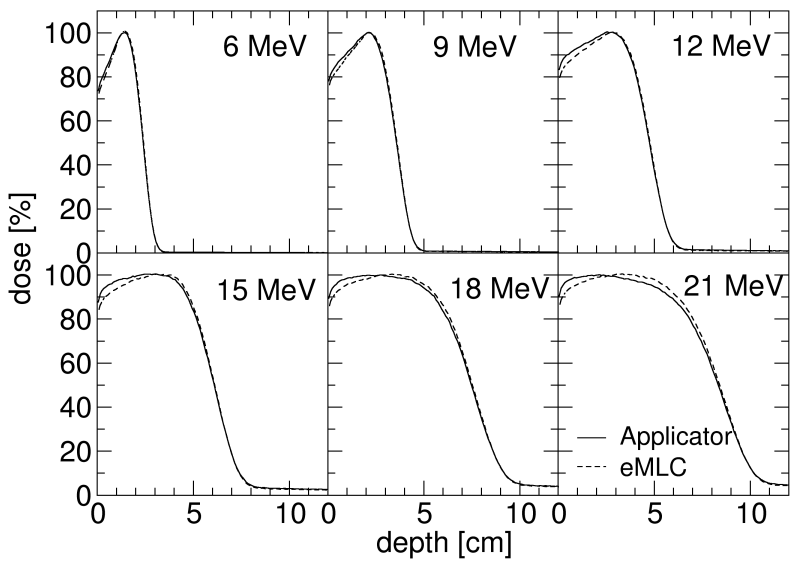

Figure 4. Comparison of central axis depth dose curves for applicator (95 cm SCD) and eMLC (81.6 cm SCD) nominal 10×10 cm^2 fields at 100 cm SSD.

The eMLC should ideally generate a penumbra similar to the applicator. Electrons scattered from the eMLC had a marginal effect on the penumbra (figure 3); a maximum of 2.5% and 2.8% of the dose in the penumbra of the 10 × 10 cm^2 field size at 6 MeV and 21 MeV, respectively. For comparison,

electrons scattered from the 10 × 10 cm^2 applicator contributed a maximum of 1.2% and 2.5% to the dose in the penumbra for the same energies. Electrons from the eMLC contributed 4.1% and 6.4% to the dose at R_{max} on the central axis (i.e. to relative output) for 6 MeV and 21 MeV, respectively. The scattered electron contribution to the dose at R_{max} for the 10 × 10 cm^2 applicator was lower, 1.1% and 3.4 % at 6 MeV and 21 MeV, respectively.

Table 3. Percentage depth dose (PDD) parameters for 10 × 10 cm^2 field and 100 cm SSD (with eMLC parameters at 90 cm SSD included in italics). R_{100}, R_{80} and R_{50} are the depths of 100, 80 and 50% of maximum dose, respectively. $D_{0.5}$ and D_x is the dose (%) at 0.5 cm depth and in the bremstrahlung tail, at depths of 5, 7, 8, 10, 12 and 13 cm for 6 – 21 MeV, respectively.

PDD parameters	Applicator						eMLC					
	energy [MeV]						*energy [MeV]*					
	6	*9*	*12*	*15*	*18*	*21*	*6*	*9*	*12*	*15*	*18*	*21*
$D_{0.5}$ [%]	84.7	86.1	90.1	95.0	96.3	97.4	82.2	83.1	86.5	90.6	92.6	93.2
							81.8	*83.5*	*86.6*	*91.0*	*94.3*	*94.5*
R_{100} [cm]	1.4	2.1	2.7	3.0	2.1	1.9	1.4	2.1	2.8	3.0	2.7	2.2
							1.4	*2.1*	*2.8*	*3.1*	*2.6*	*2.3*
R_{80} [cm]	2.02	3.05	4.07	5.17	6.25	6.85	2.06	3.09	4.11	5.25	6.38	7.06
							2.02	*3.10*	*4.12*	*5.26*	*6.34*	*6.93*
R_{50} [cm]	2.39	3.58	4.76	6.08	7.48	8.34	2.41	3.61	4.78	6.11	7.54	8.42
							2.41	*3.60*	*4.78*	*6.12*	*7.54*	*8.37*
D_x [%]	0.4	0.8	1.4	3.0	4.0	4.5	0.3	0.7	1.1	2.7	3.8	4.1
							0.3	*0.7*	*1.1*	*2.6*	*3.7*	*4.0*

The electron range in tungsten is short (only 0.5 cm for 20 MeV electrons) and the attenuation of the bremsstrahlung (x-rays) is high, therefore x-rays from the thick eMLC leaves had an insignificant contribution to the central axis dose at R_{max} (figure 3), 0.2% at 21 MeV and an order of magnitude lower at 6 MeV. This contribution is negligible compared to the x-ray dose from the treatment head, which is a maximum of 5% at 21 MeV for a 40 × 40 cm^2 field (Hogstrom et al. 2004).

For the applicator, the contribution of bremsstrahlung to the central axis dose at R_{max} was < 0.1% and 0.4% at 6 MeV and 21 MeV, respectively. The contribution was much higher at the edge of the applicator-defined field, however, a maximum of 0.1% and 2.3 % for the 6 MeV and 21 MeV electron beams, respectively. This increase is the result of bremsstrahlung creation and transmission in the 1.3 cm thick brass scraper.

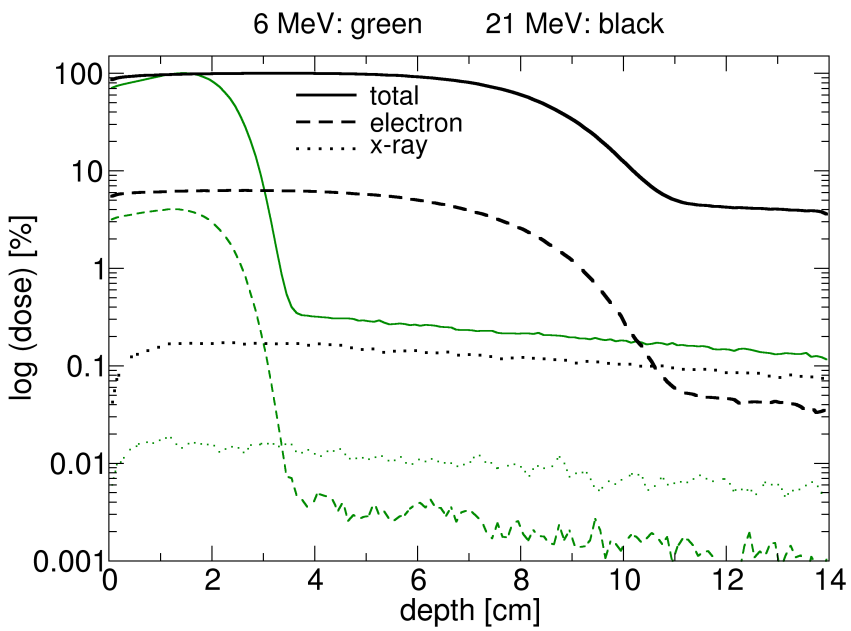

Figure 5. Percentage depth dose curves for 6 MeV and 21 MeV electron beams showing dose contribution from total electron beam (solid lines) and scattered electrons (dashed lines) and bremsstrahlung x-rays (dotted lines) from the eMLC. The bottom surface of the leaf banks were at 81.6 cm SCD, the water surface was at 100 cm SSD.

Percentage depth dose curves (normalised to nominal R_{max}) for the eMLC exhibited a lower surface dose (by 2.5 – 4.2% for 6 – 21 MeV), leading to a more deeply penetrating beam at 100 cm

SSD (R_{80}, 0.4 – 0.21 cm) than the applicator defined fields (figure 4 and table 3). The dose beyond the practical range (D_x) of the PDD was 0.1 – 0.4% lower for the eMLC, primarily the result of reduced bremsstrahlung. Table 4 also includes the eMLC PDD parameters for 90 cm SSD which are very similar to those at 100 cm SSD (within 1.7% / 0.1 cm). The only notable differences were in the build-up dose and the depth of R_{max}.

Figure 5 shows the scattered electron and bremsstrahlung dose contributed by the eMLC to the PDD at 6 MeV and 21 MeV for a 10 × 10 cm^2 field at 100 cm SSD. The bremsstrahlung component was 5.0% and 2.0% of the dose at R_x for the 6 MeV and 21 MeV beams, respectively. For the applicator collimated field, the contribution at R_x was 7.5% and 6.0%, respectively (not shown). Electrons scattered from the collimator contributed 3.6 - 5.9% of the dose at 0.5 cm and 2.8 – 3.9% at R_{80} for the eMLC at 6 – 21 MeV. The contribution was 1.7 – 5.0% at 0.5 cm depth and 0.2 – 0.6% at R_{80} for the applicator collimated field.

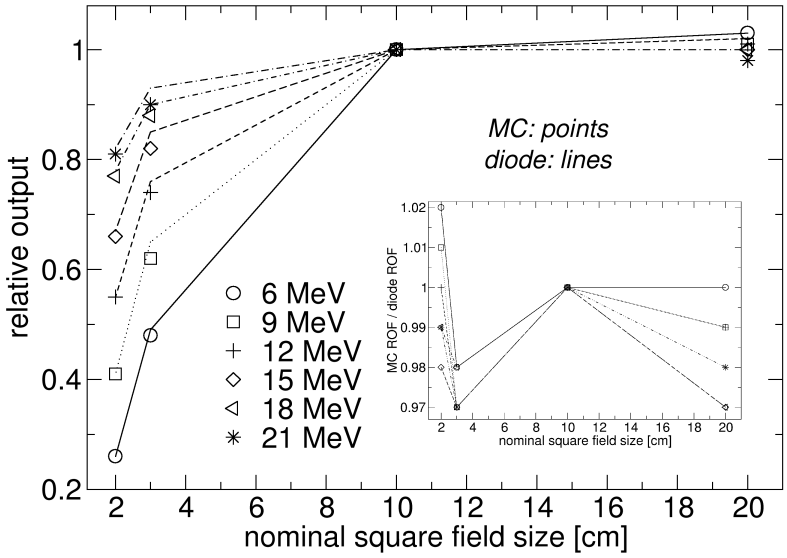

Figure 6. Monte Carlo calculated (points) and diode measured (lines) relative output factors for 2 × 2, 3 × 3, 10 × 10 and 20 × 20 cm^2 nominal field sizes collimated with eMLC (relative to 10 × 10 cm^2 field) at 81.6 cm SCD

and 100 cm SSD. The ratio of Monte Carlo calculated to diode measured relative output is shown in the inset.

Figure 6 shows the Monte Carlo calculated and diode measured relative output factors (ROF) for the 2 – 20 cm square fields at 100 cm SSD. Measurements and calculations were within 2% at 90 cm and 100 cm SSD, with several exceptions. A sharp drop in output was seen for the smaller fields (3 × 3 cm^2 → 2 × 2 cm^2) at lower beam energies. The eMLC blocks scattered electrons emanating from upstream components and, in addition, for smaller fields the primary source starts to be obscured (Chetty et al. 2007). Conversely, at the largest field size the output was lowest at 21 MeV (0.985) and highest at 6 MeV (1.030) as the result of increasing scatter from the eMLC leaves.

3.2 Leaf Resolution

It may be prudent when abutting electron fields to avoid open or shielded regions less than the penumbra width. These narrow fields could provide negligible enhancement to the dose distribution while increasing the scattered radiation in the treatment beam. It was therefore proposed that the eMLC leaf width be such that the dose below a closed leaf section is reduced to less than 50% of maximum dose (of the adjacent open sections). Figure 7 shows the dose profile at 1 cm depth for 21 MeV beam at 90 cm SSD for different numbers of eMLC leaves alternating open or closed. The dose dropped to 35.4, 9.6, 5.4 and 4.2% on the central axis blocked by combined leaf widths of 0.4, 0.8, 1.2 and 1.6 cm, respectively. For 6 MeV, the dose dropped to 99.9, 67.5, 35.9 and 19.9%, respectively, for the same configurations. The wider angular distribution of electron scattering at 6 MeV means that the 0.4 – 0.8 cm leaf widths are inadequate. An optimum leaf width of 1.02 cm was determined (for 6 – 21 MeV) based on a quadratic fit of the leaf width versus maximum dose at 1 cm depth in the shield portion of the field. For this leaf width the dose at 6 MeV was reduced to 50% of maximum and 26.2, 16.0, 10.9, 8.30 and 7.2% for 9 – 21 MeV, respectively. A thinner leaf width could be employed at the higher

energies to achieve a 50% dose reduction. The leaf width required to provide a 50% reduction in dose was 0.7, 0.6 and 0.4 cm for 9 – 15 MeV, respectively and < 0.4 cm at 18 – 21 MeV.

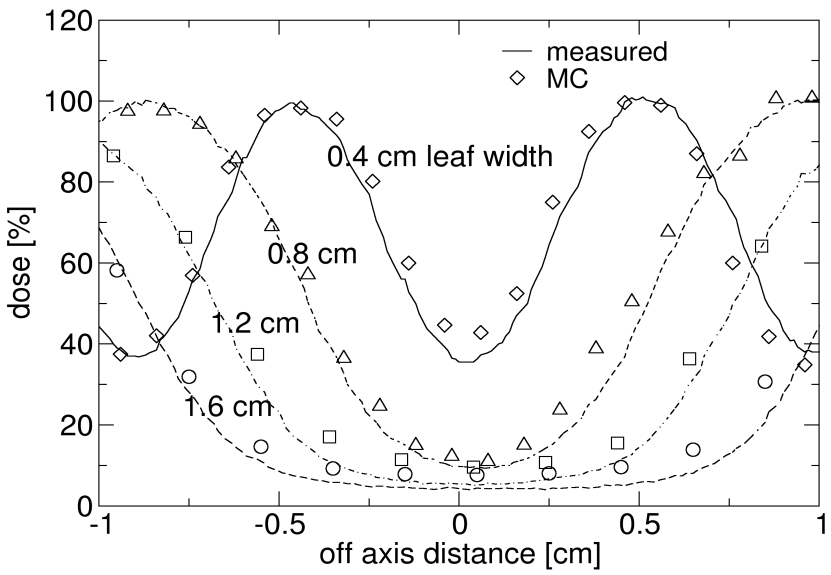

Figure 7. Dose profiles with various numbers of adjacent eMLC leaves open or closed (effective leaf widths of 0.4 , 0.8, 1.2 and 1.6 cm perpendicular to the beam) for 21 MeV and 90 cm SSD.

While limiting the leaf width may be prudent in most situations, the availability of thin leaves, conversely, may help improve the uniformity of the dose distribution at the junctions as a (thin) leaf could be added or removed on one side or the other of the junction. For example, the 18 / 21 MeV junction for the wedge field dose distribution (section 3.3) required a 2.5 mm gap. This could be approximated in the direction perpendicular to the leaf motion by having a one-leaf (0.2 cm) overlap between the fields.

3.3 Field Abutment

Matching of electron beams requires careful determination of the dose at the junction. A shift in the

location of the field junction can be used to improve the dose distribution in certain situations. Figure 8 shows the dose profile across the field junction of 6 / 9 MeV and 18 / 21 MeV matched 5 cm square fields. The dosimetric effects of field overlaps and gaps of 0.2 cm on the phantom surface are included. The wider penumbrae (6 MeV: 2.01 cm, 9 MeV: 1.49 cm) and scattering of the 6 MeV and 9 MeV beams meant that the dose across the junction was less homogeneous (max. dose – min. dose = 8.9%). There was a hotspot of 106% in the junction region when the field edges were matched. This was reduced by 10% with a 0.2 cm gap. The sharper and comparable penumbrae of the 18 MeV (0.78 cm) and 21 MeV (0.73 cm) beams resulted in a more homogeneous dose distribution in the junction region (max. dose – min. dose = 4.7%). The sharper penumbra also meant that a shift in the junction position had a larger effect on the junction dose, increasing by 13.3% and reducing by 14.2% for a 0.2 cm overlap and gap, respectively. Isodose lines for the 18 / 21 MeV abutted field are plotted in figure 9 highlighting the hot and cold spots created by the various junction configurations.

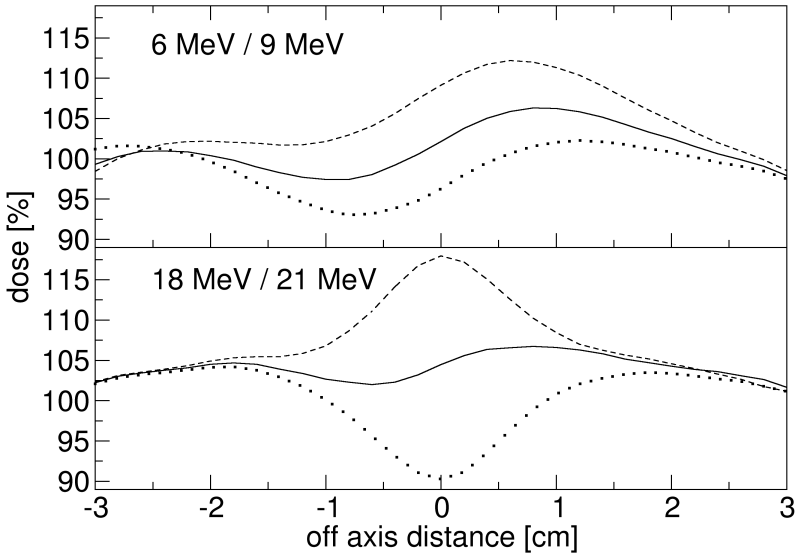

Figure 8. Monte Carlo calculated dose profiles at 1.5 cm depth for matched 6 MeV / 9 MeV and 18 MeV / 21 MeV, 5 cm square fields shaped with the eMLC (81.6 cm SCD). The dosimetric effects of a 0 cm gap (solid

lines), 0.2 cm gap (points) and 0.2 cm overlap (dashed lines) of the field junction at 100 cm SSD are shown.

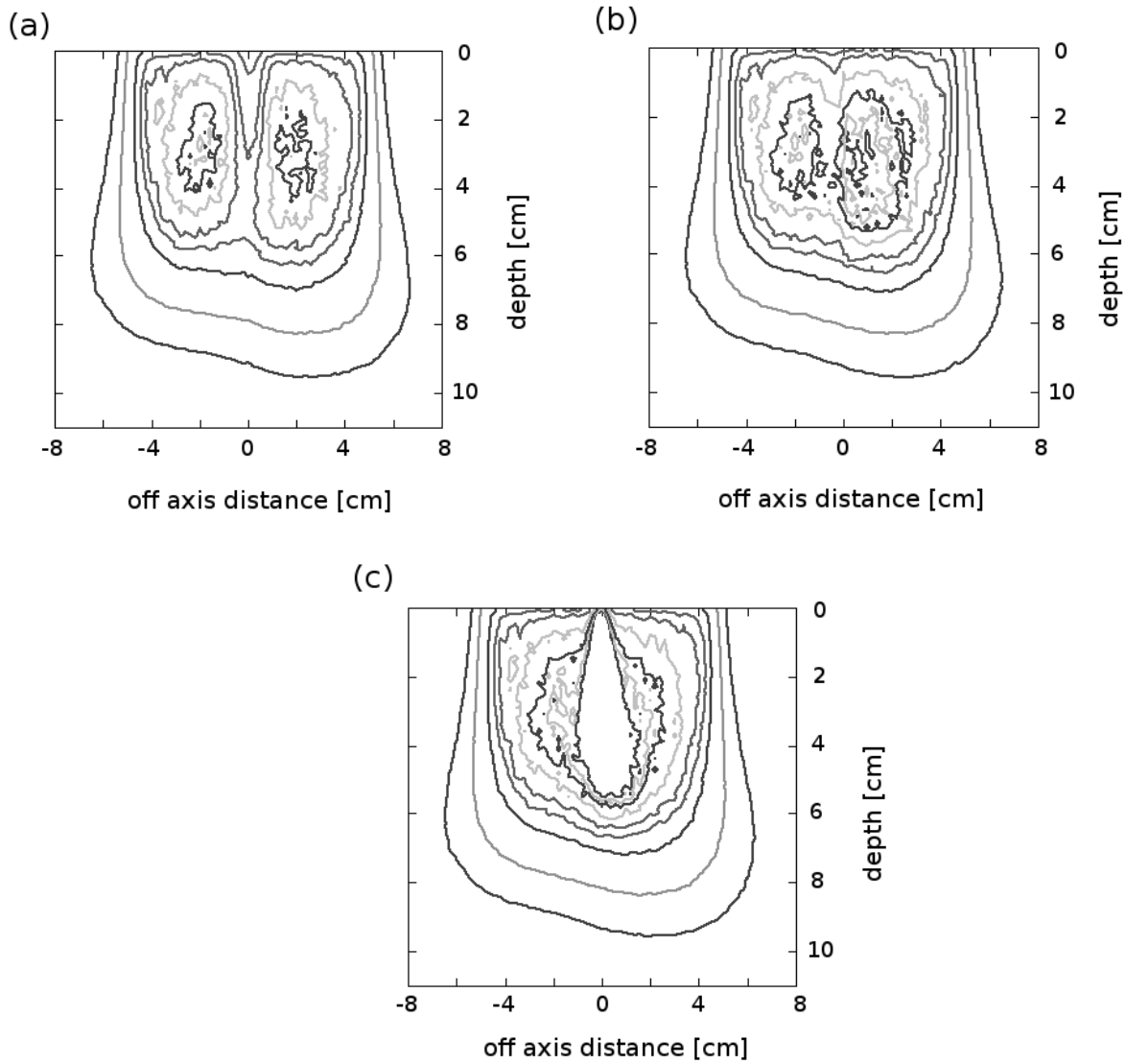

Figure 9. Monte Carlo calculated isodose lines (20, 50, 80, 90, 95, 100, 103, 105 and 107%) for 18 MeV / 21 MeV abutted 5 cm square fields shaped with the eMLC (81.6 cm SCD). The dosimetric effect of a 0.2 cm gap (a), 0.0 cm gap (b) and 0.2 cm overlap (c) at the field junction (at 100 cm SSD) are shown.

Monte Carlo calculated and diode measured profile components (6 – 21 MeV) for the wedge shaped dose distribution at 1 cm depth are compared in figure 10, demonstrating accurate calculation of the

dose and penumbrae in the segments of the energy modulated field. The wedge distribution was generated using the parameters listed in table 4 with the resultant Monte Carlo calculated dose distribution shown in figure 11. The field size and junctioning of each wedge component was adjusted to produce the greatest range in depth penetration (R_{50}) and limit the maximum hotspot to 105%. The therapeutic range (R_{80}) and depth penetration (R_{50}) varied from 2.1 – 6.8 cm

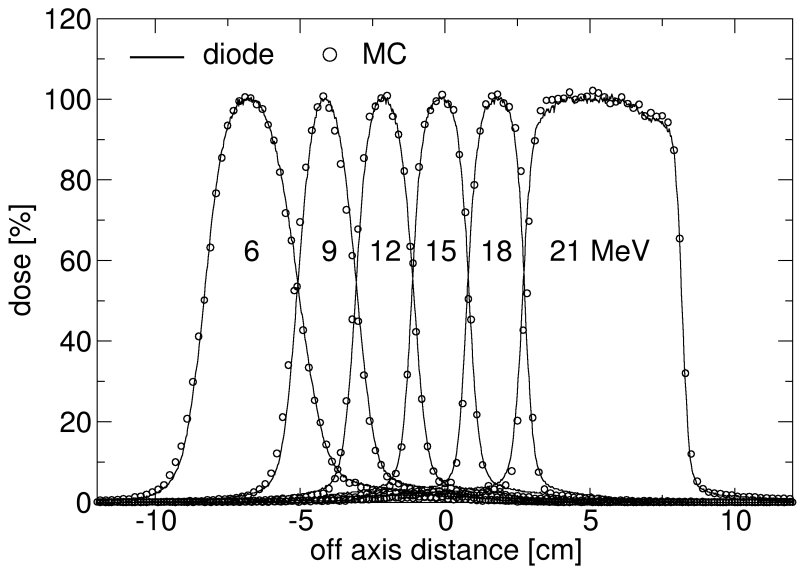

Figure 10. Comparison of Monte Carlo calculated and measured dose profiles at 1 cm depth for eMLC energy modulated wedge distribution. The eMLC was positioned at 81.6 cm SCD with a SSD of 100 cm.

and 2.5 – 8.2 cm, respectively. The 21 MeV beam utilised a large field width (5.15 cm) to limit the effects of loss of electronic equilibrium and consequently, achieve maximum depth penetration. The penumbrae for the field segments used in the wedge shaped dose distribution showed a decrease in width, from 2.1, 1.8, 1.8, 1.5, 1.0 and 0.9 cm for the nominal 10 × 10 cm^2 field (table 2) to 1.7, 1.5, 1.4, 1.2, 0.8 and 0.8 cm for 6 – 21 MeV, respectively. It was necessary to have a gap at the field junctions for the lower energies and an overlap at the higher energies (table 4). The 6 MeV and 9 MeV junction

required a 0.25 cm gap, while 9 MeV and 12 MeV junction required a 0.05 cm gap. The high energy beam junctions were each overlapped (with there corresponding lower energy abutted beam) by 0.1 cm (15 MeV) – 0.25 cm (21 MeV). The wedge distribution demonstrates the range in depth penetration available with energy modulation at 6 – 21 MeV and highlights the field matching challenge which proved to be particularly challenging at lower energies.

Table 4. MCRTP calculated eMLC energy-modulated wedge profile parameters at 100 cm SSD. Field junctions and relative weighting was adjusted so the maximum hotspot did not exceed 105%.

Energy [MeV]	Field size [cm]	Field offset [cm]	Neg. eMLC bank [cm]	Pos. eMLC bank [cm]	Gap [-] or Overlap [+]	Relative weight [%]
6	2.85	-8.71	-10.14	7.29	-	99
9	3.15	-5.48	-7.03	-3.93	-0.25 cm	84
12	3.05	-2.45	-3.98	-0.92	-0.05 cm	85
15	3.20	0.58	-1.02	2.18	+0.10 cm	84
18	3.15	3.66	2.08	5.24	+0.10 cm	92
21	5.15	7.56	4.99	10.14	+0.25 cm	97

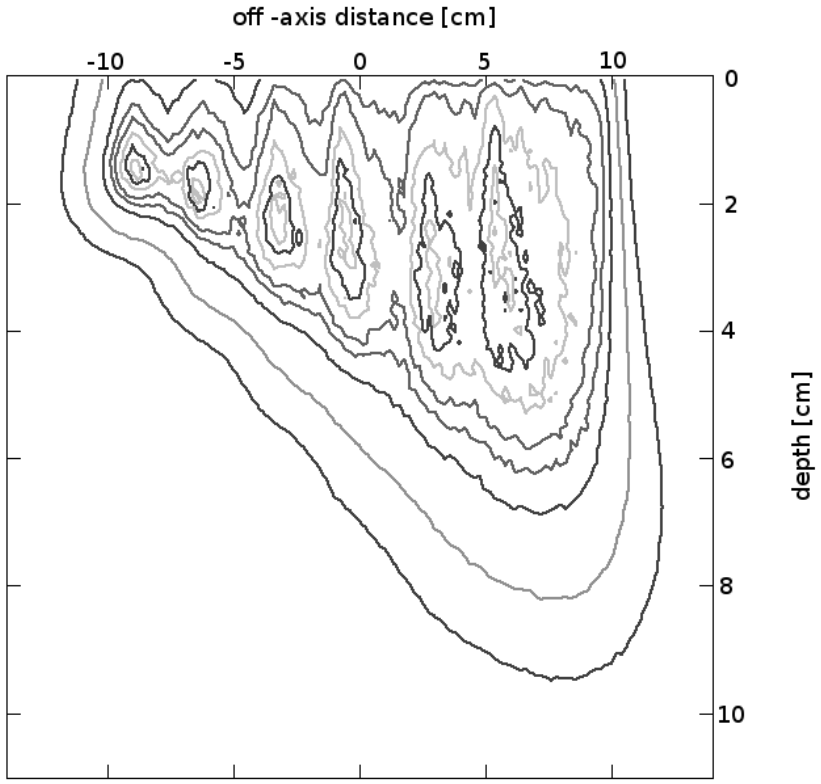

Figure 11. Monte Carlo calculated isodose distribution for eMLC (6 - 21 MeV) energy modulated wedge. SCD and SSD were 81.6 cm and 100 cm, respectively. The 20, 50, 80, 90, 95, 100, 103 and 105% isodose lines are displayed. The parameters used to generate the dose distribution are listed in table 4.

3.4 Patient Plan

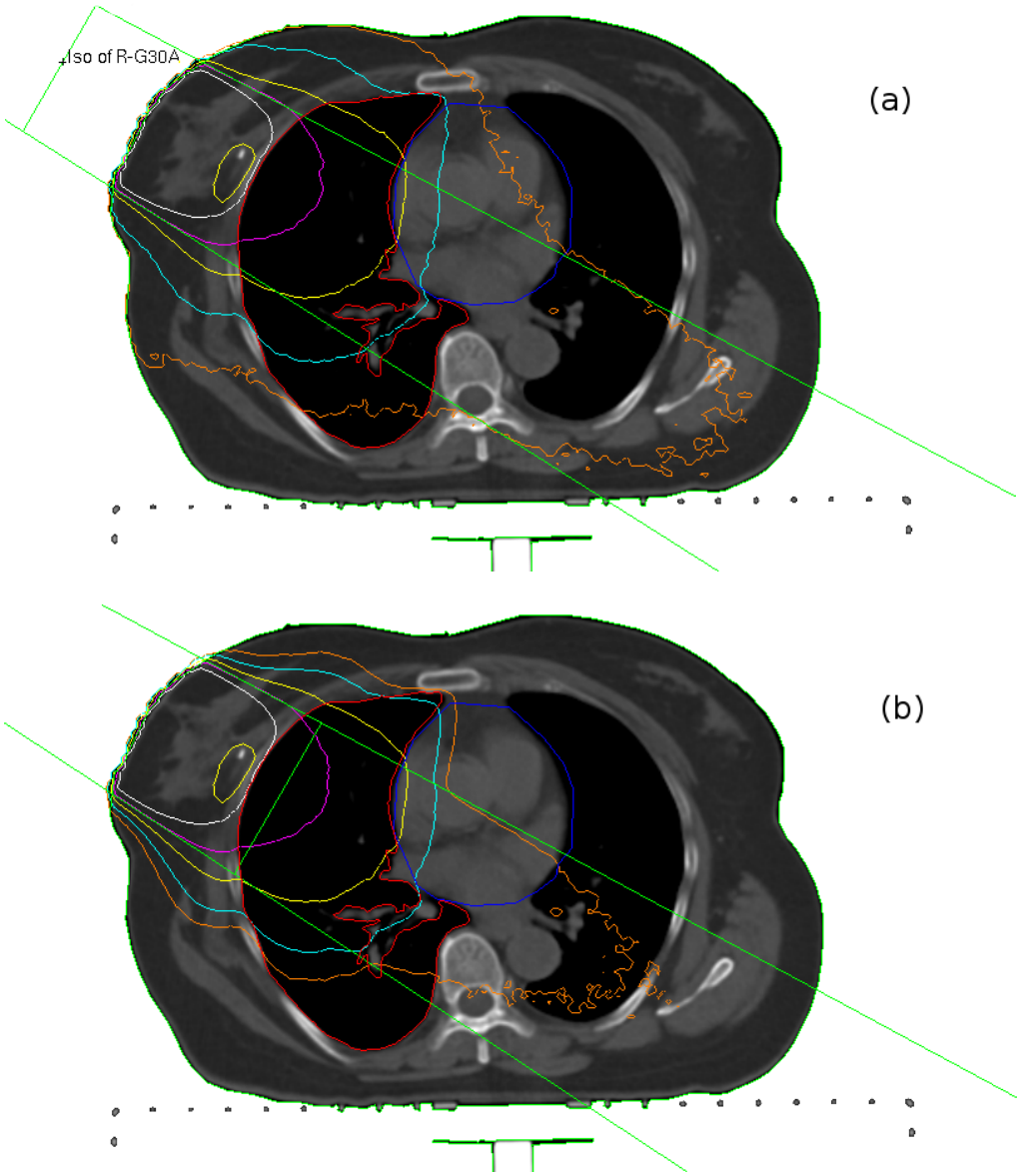

Figure 12. Monte Carlo calculated isodose lines displayed in PlanUNC for (a) conventional applicator and (b) eMLC isocentric, electron breast boost using an 18 MeV electron beam. The 2, 5, 20, 50 and 80% isodose lines are shown. Plan parameters are listed in table 1.

The Monte Carlo calculated dose distributions for the conventional applicator / SSD and eMLC isocentric electron breast boost plans are shown on patient CT in figure 12 (for the applicator plan isocentre CT slice). Bremsstrahlung generated in and transmissed through the 1.3 cm thick Cerrobend

insert used with the applicator resulted in a wider lateral extension of the 2% and 5% isodose lines. Subsequently, the 2% isodose line encompassed a larger volume of the heart. The 7 cm thick eMLC leaves effectively eliminated bremsstrahlung in the shielded areas and the lateral extension of the 2% and 5% isodose lines was constricted.

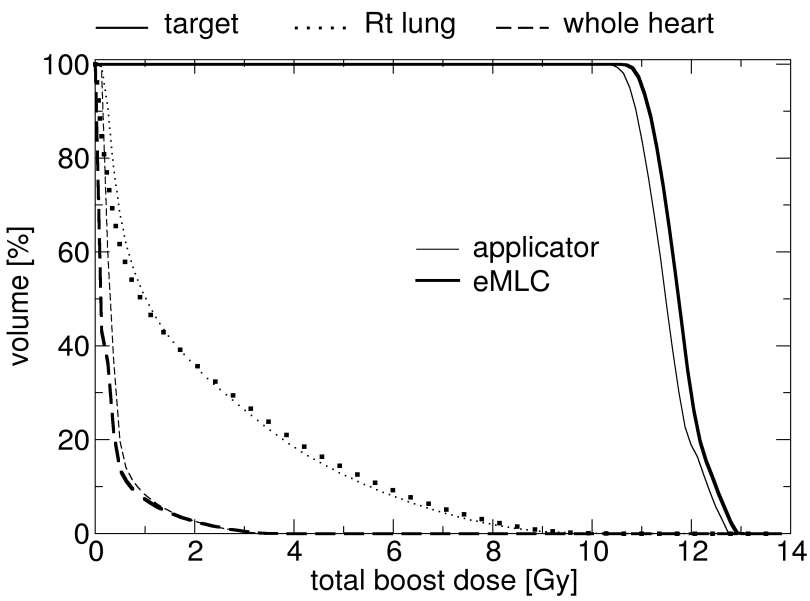

Figure 13. Dose-volume histograms (DVH) for conventional applicator and eMLC (concomitant) isocentric electron breast boost using an 18 MeV electron beam. The DVH for the target, Rt lung and whole heart contours are shown. Plan parameters are listed in table 1.

The mean dose to the target, right lung and whole heart was 91.8%, 15.8% and 3.0% for the applicator and 93.7%, 15.8% and 2.0%, for the eMLC plan, respectively. The DVHs for these structures are compared in figure 13. $D95_{CTV}$ was 107.5% and 110.1% for the standard applicator and eMLC plans, respectively. $V20_{lung}$ was 510.4 cm^3 and 515.9 cm^3, while $V10_{heart}$ was 66.7 cm^3 and 58.6 cm^3, for the applicator and eMLC plans, respectively.

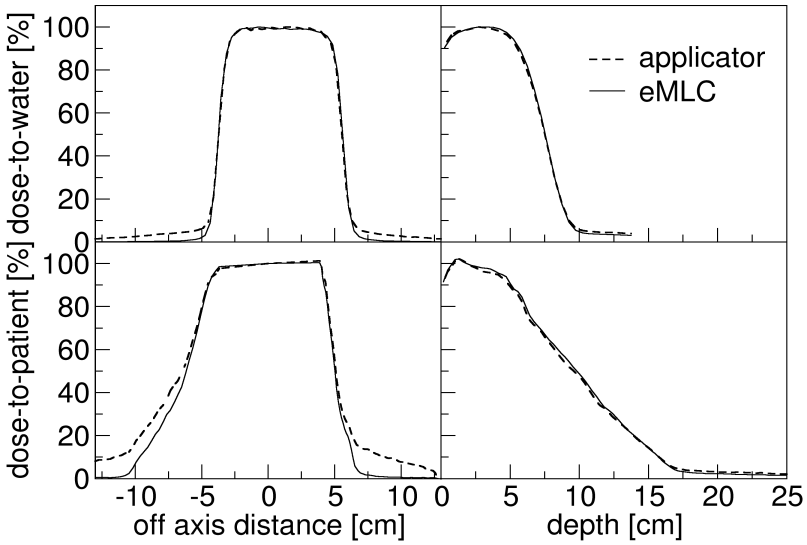

Figure 14. Simulated dose profiles and percentage depth dose (PDD) curves for the conventional applicator and eMLC isocentric plans delivered to the water phantom (top row) and the patient (lower row).

The Monte Carlo calculated (20%, 50% and 80%) isodose lines for the applicator and eMLC plans delivered to a water phantom agreed to within 0.25 cm. Figure 14 displays the R_{max} dose profiles and central axis PDD for the two plans. The penumbral width for the eMLC (0.86 cm) and applicator (0.83 cm) plans, which employed the same airgap, agreed to 0.03 (± 0.03) cm. Scattered electrons from the eMLC did not degrade the penumbra. The reduction in dose due to low bremsstrahlung under the eMLC leave banks can be seen in the umbral region for the eMLC plan. The differences in R_{80}, R_{50} and D_x on the central axis were 0.13 cm, 0.06 cm and 0.9% for the two plans. Figure 14 includes dose profiles and central axis PDD for the patient. The increased bremsstrahlung for the applicator plan led to the differences seen in the applicator and eMLC dose profiles. The percentage depth dose curves were similar with differences of 0.10 cm, 0.20 cm and 0.9% in R_{80}, R_{50} and the dose at 20 cm depth, respectively.

4 SUMMARY AND CONCLUSIONS

An extendable multi-leaf collimator (eMLC), which could be positioned at 59 – 95 cm from the source, was investigated for collimation of clinical electron beams. The eMLC was modelled using the Monte Carlo code EGSnrc and validated against percentage depth dose, dose profile and relative output measurements, showing agreement to 2% / 2 mm. The penumbra for a 10 × 10 cm^2 field was up to 0.12 cm narrower for the applicator with a 5 cm air gap compared to the eMLC penumbra at 81.6 cm SCD (18 cm air gap). The main effect on the percentage depth dose curve was a reduction in dose in the build-up region, of up to 4.2% at 0.5 cm depth, with a 0.04 – 0.21 cm shift in R_{80} towards deeper beam penetration. These results are similar to those reported by a previous study (Gauer et al. 2008), however, it is important to note that the thicker MLC employed in the current study did not introduce significant dose profile or PDD degrading collimator scatter. Additionally the eMLC dose profile and PDD parameters at 90 cm SSD - relevant to isocentric treatment delivery - were found to be in good agreement with the applicator parameters.

Scatter from the eMLC contributed 4.0 - 6.3% (6 - 21 MeV) to the dose at the depth of maximum dose, while the 7 cm thick leaves effectively eliminated bremsstrahlung leakage. Field junctioning was a challenge at lower energies due to the wider penumbrae and angular distribution of electron scattering. A Monte Carlo calculated wedge shaped dose distribution consisting of 6 – 21 MeV matched electron fields utilising the entire available field width of the eMLC exhibited a variation in therapeutic range of 2.1 – 6.8 cm.

An isocentric eMLC breast boost plan showed similar target coverage and dose to organs-at-risk as the conventional applicator and fixed source-to-surface distance approach. Dose to the whole heart was reduced as a result of the very low bremsstrahlung contamination from the thick eMLC leaves. Thick leaves may be advantageous for intensity modulated electron therapy techniques where the

summation of bremsstrahlung dose from multiple fields can be a concern. The dose profiles and percentage depth dose curves for the eMLC and applicator exhibit very similar characteristics when the airgap between the collimator and patient surface is the same.

Monte Carlo simulation can accurately account for the eMLC and patient in dose calculation for treatment planning. Potential benefits of the eMLC include (i) faster delivery (no room re-entry to insert applicator), (ii) reduction in risk of positioning errors (using a single isocentre and no couch repositioning) and (iii) a practical method of modulated delivery.

References

Alexander A, Soisson E, Hijal T, Sarfehnia A and Seuntjens J 2011 Comparison of modulated electron radiotherapy to conventional electron boost irradiation and volumetric modulated photon arc therapy for treatment of tumour bed boost in breast cancer Radiotherapy and Oncology 100 253-258

Al-Yahya K, Verhaegen F and Seuntjens J 2007 Design and dosimetry of a few leaf electron collimator for energy modulated electron therapy Med. Phys. 34 (12) 4782-4791

Bartelink H, Horiot J-C, Poortmans P, Struikmans H, Van den Bogaert W, Barillot I, Fourquet A, Borger J, Jager J, Hoogenraad W, Collette L and Pierart M 2001 Recurrence Rates after Treatment of Breast Cancer with Standard Radiotherapy with or without Additional Radiation New England Journal of Medicine 345 (19) 1378-1387

Chetty I J et al 2007 Report of the AAPM Task Group No. 105: issues associated with clinical implementation of Monte Carlo-based photon and electron external beam treatment planning Med. Phys. 34 4818–53

Coleman J, Park C, Villarreal-Barajas J E, Petti P and Faddegon B 2005 A comparison of Monte Carlo and Fermi-Eyges-Hogstrom estimates of heart and lung dose from breast electron boost treatment International Journal of Radiation Oncology

Biology Physics 61 (2) 621-628

Eldib A, ELGohary M, Fan J, Jin L, Li J, Ma C, Elsherbini N 2010 Dosimetric characteristics of an electron multileaf collimator for modulated electron radiation therapy J. Appl. Clin. Med. Phys. 11 (2) 5-22

Faddegon B A, Balogh J, Mackenzie R and Scora D 1998 Clinical considerations of Monte Carlo for electron radiotherapy treatment planning Radiat. Phys. Chem. 53 217–27

Faddegon B A, Sawkey D L, O'Shea T P, McEwen M and Ross C 2009 Treatment head disassembly to improve the accuracy of large electron field simulation Med. Phys. 36 4577–91

Fraser D J, Wong P, Sultanem K and Verhaegen F 2010 Dosimetric evolution of the breast electron boost target using 3D ultrasound imaging Radiotherapy and Oncology 96 (2) 185-91

Gauer T, Albers D, Cremers F, Harmansa R, Pellegrini R and Schmidt R 2006 Design of a computer-controlled multileaf collimator for advanced electron radiotherapy Phys. Med. Biol. 51 5987

Gauer T, Sokoll J, Cremers F, Harmansa R, Luzzara M and Schmidt R 2008 Characterization of an add-on multileaf collimator for electron beam therapy Phys. Med. Biol. 53 1071

Gauer T, Engel K, Kiesel A, Albers D and Rades D 2010 Comparison of electron IMRT to helical photon IMRT and conventional photon irradiation for treatment of breast and chest wall tumours Radiotherapy and Oncology 94 313-318

Hogstrom K R, Boyd R A, Antolak J A, Svatos M, Faddegon B and Rosenman J G 2004 Dosimetry of a prototype retractable eMLC for fixed-beam electron therapy Med. Phys. 31 443

Jin L, Ma C-M, Fan J, Eldib A, Price R A, Chen L, Wang L, Chi Z, Xu Q, Sherif M and Li J S 2008 Dosimetric verification of modulated electron radiotherapy delivered using a photon multileaf collimator for intact breasts Phys. Med. Biol. 53 (21)

6009

Klein E E, Vicic M, Ma C-M, Low D L and Drzymala R E 2008 Validation of calculations for electrons modulated with conventional photon multileaf collimators Phys. Med. Biol. 53 1183

Klein E E, Mamalui-Hunter M and Low D A 2009 Delivery of modulated electron beams with conventional photon multi-leaf collimators Phys. Med. Biol. 54 327

Lee M C, Jiang S B and Ma C-M 2000 Monte Carlo and experimental investigations of multileaf collimated electron beams for modulated electron radiation therapy Med. Phys. 27 2708

Ma C M and Jiang S 1999 Monte Carlo modelling of electron beams from medical accelerators Phys. Med. Biol. 44 157–89

O'Shea T P, Foley M J and Faddegon B A 2011 Accounting for the fringe magnetic field from the bending magnet in a Monte Carlo accelerator treatment head simulation Med. Phys. 38 (6) 3260-3269

Rogers D W O, Faddegon B A, Ding G X, Ma C M and We J 1995 BEAM: a Monte Carlo code to simulate radiotherapy treatment units Med. Phys. 22 503–24

Schreiber E, Tracton G, and Chaney E 2006 Tools for Integrating Monte Carlo Dose Engines with a Radiotherapy Planning System Med. Phys. 33 2146

Steel J, Stewart A, and Satory P 2009 Matching extended-SSD electron beams to multileaf collimated photon beams in the treatment of head and neck cancer Med. Phys. 36 4244

Surucu M, Klein E E, Mamalui-Hunter M, Mansur D B and Low D A 2010 Planning tools for modulated electron radiotherapy Medical Physics 37 (5) 2215-2224